Physics and Imaging in Radiation Oncology 25 (2023) 100419

Contents lists available at ScienceDirect

Physics and Imaging in Radiation Oncology

journal homepage: www.sciencedirect.com/journal/physics-and-imaging-in-radiation-oncology

Original Research Article

A method for beam's eye view breath-hold monitoring during breast volumetric modulated arc therapy

M.A. Carr [a,b,*], M. Gargett [a,c], C. Stanton [a], B. Zwan [d], H.L. Byrne [e], J.T. Booth [a,b]

[a] Northern Sydney Cancer Centre, Royal North Shore Hospital, Sydney, New South Wales, Australia
[b] Institute of Medical Physics, School of Physics, The University of Sydney, Sydney, New South Wales, Australia
[c] School of Health Sciences, Faculty of Medicine and Health, The University of Sydney, Sydney, New South Wales, Australia
[d] Central Coast Cancer Centre, Gosford Hospital, Gosford, New South Wales, Australia
[e] ACRF Image-X Institute, Faculty of Medicine and Health, The University of Sydney, Sydney, New South Wales, Australia

ARTICLE INFO

Keywords:
BEV monitoring
Breast VMAT
DIBH
Deep inspiration breath-hold
Electronic portal imaging device
Cine EPID
Intrafraction motion
Chest wall

ABSTRACT

Background and purpose: Deep inspiration breath-hold (DIBH) is a technique that is widely utilised to spare the heart and lungs during breast radiotherapy. In this study, a method was developed to validate directly the intrafraction accuracy of DIBH during breast volumetric modulated arc therapy (VMAT) via internal chest wall (CW) monitoring.

Materials and methods: In-house software was developed to automatically extract and compare the treatment position of the CW in cine-mode electronic portal image device (EPID) images with the planned CW position in digitally reconstructed radiographs (DRR) for breast VMAT treatments. Feasibility of this method was established by evaluating the percentage of total dose delivered to the target volume when the CW was sufficiently visible for monitoring. Geometric accuracy of the approach was quantified by applying known displacements to an anthropomorphic thorax phantom. The software was used to evaluate (offline) the geometric treatment accuracy for ten patients treated using real-time position management (RPM)-guided DIBH.

Results: The CW could be monitored within the tangential sub-arcs which delivered a median 89% (range 73% to 97%) of the dose to target volume. The phantom measurements showed a geometric accuracy within 1 mm, with visual inspection showing good agreement between the software-derived and user-determined CW positions. For the RPM-guided DIBH treatments, the CW was found to be within ±5 mm of the planned position in 97% of EPID frames in which the CW was visible.

Conclusion: An intrafraction monitoring method with sub-millimetre accuracy was successfully developed to validate target positioning during breast VMAT DIBH.

1. Introduction

Adjuvant breast radiotherapy is an integral component of the treatment of breast cancer, reducing recurrence and improving survival rates [1]. As radiation dose to the heart has been linked to an increase in the risk of major coronary events [2], deep inspiration breath-hold (DIBH) is utilised for the majority of left-sided breast cancer patients to improve heart sparing [3]. Most implementations of DIBH involve the use of a surrogate (chest surface, a marker block or volume of air inhaled), introducing uncertainty into the patient's positioning and potentially increasing geometric planning target volume (PTV) margins [4–6]. Direct monitoring of internal anatomic structures can reduce surrogacy errors, therefore improving the targeting accuracy and precision and minimising dosimetric errors associated with breath-hold level uncertainty [7].

In contrast to tangential three-dimensional conformal radiotherapy (3D-CRT) and intensity-modulated radiotherapy (IMRT) techniques of breast radiotherapy, volumetric modulated arc radiotherapy (VMAT) provides more degrees of freedom with regards to beam parameter optimisation in order to achieve improved target dose conformity [8,9]. This is particularly important for improving the balance of target coverage and organ-at-risk sparing, especially where short fractionation schemes (40.05 Gy in 15 fractions, 26 Gy in 5 fractions) and multi-dose level prescriptions (simultaneous integrated boost) are employed. Breast

* Corresponding author at: Department of Radiation Oncology, Royal North Shore Hospital, Northern Sydney Cancer Centre, Level 1, Royal North Shore Hospital, Reserve Road, St Leonards, NSW, 2065, Australia.
E-mail address: Michael.Carr@health.nsw.gov.au (M.A. Carr).

https://doi.org/10.1016/j.phro.2023.100419
Received 8 September 2022; Received in revised form 19 January 2023; Accepted 20 January 2023
Available online 25 January 2023

VMAT is traditionally associated with increased low-dose wash, however recently the use of knowledge-based planning has been shown to achieve the low-dose wash benchmark of base-tangential methods [10,11] significantly increasing its potential application in breast radiotherapy treatment.

Beam's eye view (BEV) imaging using an electronic portal image device (EPID) can allow direct monitoring of internal anatomy during radiotherapy using equipment available on a standard linear accelerator (linac), without additional imaging dose. Visualisation of the chest wall (CW) in BEV images collected on a C-arm linac during traditional tangential open field radiotherapy has been demonstrated [4,12–14]. Extracting the CW position for tangential IMRT delivery is challenging because the MLC will move and obscure the feature. For VMAT delivery there are further challenges as the anatomy projected in the BEV will change with gantry angle, and treatment planning system (TPS) optimisers typically provide MLC patterns that obscure a larger portion of the BEV. One group [15] has utilised EPID imaging on a closed-bore linac for analysing breast VMAT DIBH treatments at a single gantry angle with manual registration to extract the CW position. This approach is limited as monitoring of the CW position is only performed for a small number of time points during the treatment and the reported CW position may be subject to inter-user variability during manual registration.

The aim of this study was to determine the feasibility and accuracy of a time-resolved BEV-based CW monitoring software developed for breast VMAT on both C-arm and closed bore linacs.

2. Methods and Materials

2.1. Patient cohort

The selected cohort of ten breast VMAT patients included a representative range of patients receiving treatment to the whole breast or chest wall (post mastectomy). Further patient details are included in Supplementary Table 1. Consent for the use of patient data was obtained with ethics approval (ref LNR/15/HAWKE/355).

Two Varian linac platforms were used to treat patients in this study; TrueBeam (Millennium 120 leaf MLC, three patients) and Halcyon (SX2 114 leaf MLC, seven patients). All patients were immobilised in the supine position lying flat on a wingboard (arms raised above head) and planned with a 5 mm CTV-PTV margin, with the CTV defined per ESTRO consensus guidelines [16]. VMAT plans were generated in the Eclipse treatment planning system (TPS) v15.6 (Varian Medical Systems, Palo Alto, CA, USA) using knowledge-based planning [10]. A standalone real-time position management (RPM; Varian Medical Systems) implementation was used for DIBH respiratory gating on the Halcyon, and the integrated Respiratory Gating for TrueBeam (both of which will henceforth be referred to as RPM). Daily cone beam CT (CBCT) image guidance was used, with the CW as the primary match structure.

For these patients, EPID imaging data from a total of 29 fractions (78 treatment arcs) were captured using a frame grabber and iTools Capture (Varian Medical Systems) research software located on standalone research computers. Cine EPID images with pixel width at isocentre 0.3 mm were captured at 15 Hz on the TrueBeam linac (~1.2 frames per degree), and at 20 Hz on the Halcyon linac (~1.6 frames per degree). The source to image distance was 160 cm for the TrueBeam and 154 cm for the Halcyon. Gantry angles are reported in Varian IEC 601–2-1 coordinate system (Supplementary Fig. 1).

2.2. Chest wall monitoring software

The chest wall monitoring software was developed using Matlab (Version R2020a; MathWorks Inc.). The DICOM-RT treatment plan, structure set, reference CT scan (for DRR generation) and EPID images captured during treatment were the required inputs of the software. In-house software was used to generate DRRs via raytracing. The DRRs were spaced every 0.25° around the treatment arc, resulting in 881 DRRs reconstructed for each 220° arc. MLC (and jaw) positions were interpolated from the corresponding control points in the treatment plan to match the angular spacing of the DRRs.

To locate the planned position of the CW, horizontal line profiles, spaced 2 mm apart, were extracted from each DRR (Fig. 1(a)–(b)). In each profile, an initial estimate of the position of the CW was automatically determined by locating the boundary of the lung structure in the patient's DICOM structure set. The CW was then located by finding the pixel with peak intensity in a region around this initial estimate. The expected position of the MLC was compared to the position of the CW in the isocentric plane projected at the corresponding gantry angle. This allowed for an estimate of the visibility of the CW during treatment (Fig. 1(c)).

To locate the CW during treatment, each intrafraction EPID image was paired with the DRR generated at the closest gantry angle. Centre pixels of both images were then overlaid to place both the EPID image and corresponding DRR in the same coordinate system. Horizontal profiles were extracted from the EPID image at positions that correspond to those from the DRR. In each profile, an initial search window of ±15 mm was centred on the position of the CW that had been located in the corresponding profile from the DRR. The position of the MLC was extracted from the header to indicate whether the MLC entered this search window. If any leaf had entered the search window for a profile, then that profile was discarded, otherwise, the CW was located by finding the peak pixel intensity in the search window. After this process had been applied to all EPID frames, a second pass was performed. The position of the CW found in the first pass was used to estimate the CW position in neighbouring profiles and EPID frames, with the search window being reduced to ±6 mm to allow for a greater number of the horizontal line profiles to be utilised.

The CW displacement was determined as the distance between the CW's planned position (from the DRR images) and the measured position during treatment (from the EPID images). This was calculated for each individual profile where the CW was detected in both the DRR and the EPID images. The mean CW displacement was defined as the average CW displacement for all these profiles within an EPID frame. Mean CW displacements were not reported where EPID images contained less than three profiles.

2.3. Feasibility of BEV-based chest wall monitoring for VMAT

The chest wall monitoring software was utilised to assess the visibility of the CW for each patient. The CW was considered to be visible at a given gantry angle if, along at least three horizontal profiles, the CW in the DRR was found to be inside the beam aperture by a margin of at least 6 mm. The 6 mm threshold was chosen to account for realistic deviations in the treatment position of the CW from its planned position. The percentage of gantry angles for which the CW was considered visible was calculated for each treatment arc.

The proposed monitoring method will be considered feasible if the gantry angles at which the CW is visible correspond to angles with the highest dose contribution to the PTV, and vice versa. The percentage of dose delivered to the PTV as a function of gantry angle was estimated by calculating the mean dose delivered to either the CW PTV or breast PTV in subarcs of the treatment fields. Treatment plans were split into 20 subarc lengths of 11° per field. The percentage of gantry angles in which the CW was visible in each subarc was calculated and weighted by the mean dose to PTV in the same subarc. This allowed estimation of the percentage of dose to the PTV that could be monitored during treatment.

2.4. Accuracy of chest wall monitoring software in phantom geometry

A dual-arc clinical VMAT treatment plan for a left-sided breast patient was transferred onto the CT data set of an anthropomorphic thorax phantom (Radiology Support Devices Inc., USA) to estimate residual

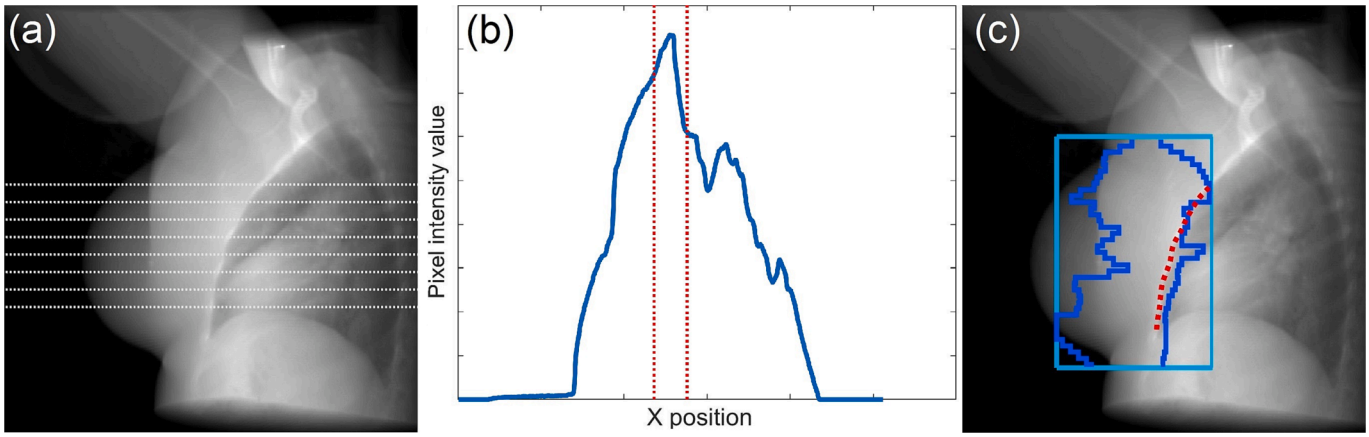

Fig. 1. (a) Horizontal line profiles extracted from a patient DRR image at gantry angle 140°. (b) The intensity values of one of the extracted profiles. The CW is located at the peak pixel value that is found in the search window (red). (c) The resulting CW delineation (red) with MLC (blue) and jaw (light blue) positions superimposed. (For interpretation of the references to colour in this figure legend, the reader is referred to the web version of this article.)

system uncertainty. CBCT imaging was used to align the phantom CW to the reference position. Cine EPID data was then captured as the treatment arcs were delivered.

The linac couch was used to shift the phantom by 5 mm in known directions along the transverse plane in order to simulate CW displacements in different directions (see Supplementary Fig. 2). The magnitude and direction of each shift was verified via CBCT imaging. The chest wall monitoring software was used to calculate the time-resolved mean CW displacement for each known phantom shift. A consequence of the use of planar EPID images was that only the component of the CW displacement in the plane orthogonal to the direction of the treatment beam was measured. For a static couch shift, the CW displacement that was expected to be measured varied as a function of the gantry angle at which the EPID image is captured. If the couch shifted the phantom at an angle of α in the anterior-posterior (AP) and left–right (LR) plane, with a magnitude of R, then the CW displacement expected to be measured in an EPID image captured at a gantry angle of θ, $d_{CW}(\theta)$, was given (Supplementary Fig. 3) by:

$$d_{CW}(\theta) = R\sin(\theta - \alpha) \quad (1)$$

The accuracy of the breast VMAT analysis software was defined as the root mean square error (RMSE) of the difference of the expected and measured mean CW displacements.

2.5. Determination of DIBH accuracy for a patient cohort

The chest wall monitoring software was applied offline (Supplementary Vid. 1) and the mean CW displacement was calculated. The accuracy of the software when applied to a patient cohort was assessed qualitatively by means of visual inspection of the software-derived CW position overlaid on the corresponding DRR or EPID image. To assess accuracy of the RPM-guided treatment, the percentage of EPID frames with mean CW displacement within the ±5 mm PTV margin was calculated per patient, and over the entire cohort.

To understand the clinical impact of setup errors and intrafraction motion detected by the software, a dosimetric analysis was performed for the single treatment fraction with the greatest observed mean CW displacement in the 20° subarcs centred at the tangential gantry angles of 130° and 310°. This provided an estimate of the dosimetric impact on target and organ at risk dose in the theoretical worst case of a systematic error. The change in dose was modelled via an isocentre shift in the TPS, with the isocentre position moved by the magnitude of the mean CW displacement in the direction orthogonal to the tangential gantry angles. A rigid relationship between the CW and the target and OAR structures was assumed. The prescribed dose to the target for this case was 50 Gy in 25 fractions. The change in minimum dose to 95% ($D_{95\%}$) of the CTV, ipsilateral lung volume receiving 10% ($V_{10\%}$) and 40% ($V_{40\%}$) of the prescribed dose, and mean heart dose (MHD) were calculated for the fraction.

3. Results

3.1. Feasibility of EPID-based chest wall monitoring for VMAT

The CW was found to be visible at 66% (median; range 42% to 93%) of gantry angles. The CW could consistently be extracted in the tangential subarcs (see Supplementary Fig. 1), located at the beginning and end of the arc (Fig. 2(a)). The percentage of delivered dose to the PTV was also greatest in the tangential subarcs (Fig. 2(b)). Across the 27 treatment arcs, a median 89% (range 73% to 97%) of the dose delivered to the PTV occurred at angles where the CW was detectable and not obscured by the MLC.

3.2. Accuracy of chest wall monitoring software in phantom geometry

Each shift in the position of the phantom was detected with an RMSE of no more than 0.5 mm, with the 5th and 95th percentile errors within a millimetre, indicating that the chest wall monitoring had an accuracy better than 1 mm (Table 1).

3.3. Determination of DIBH accuracy for a patient cohort

Overall, the CW was sufficiently visible in 15,698 of the captured EPID images. Visual audit of each patient's software-derived CW position showed good agreement in all DRR images and all but a small portion (less than 2%) of the EPID images. As such, the software-derived CW position was regarded as the true position.

The CW displacement reported for the patient cohort, shown in Figs. 3 and 4, is representative of the accuracy of the RPM-guided treatment delivery. The median CW displacement over all 10 patients was found to be 0.3 mm (range −7.1 mm to 7.0 mm). The CW was found to be within ±5 mm of its planned position in 97% of EPID images for which the mean CW displacement could be measured (Fig. 3(a)). Per patient, the CW was found to be within ±5 mm of the planned position from 79% to 100% of the time (Fig. 4).

Patient 04 had the largest median CW displacement (2.5 mm anterolaterally), which was clearly visualised in the EPID images (Fig. 3(b)–(c)). The fraction of patient 04 with the greatest mean CW displacement in the tangential subarcs, 6.5 mm, resulted in a reduction of target coverage, with CTV $D_{95\%}$ decreased from 99% to 96%. Ipsilateral lung

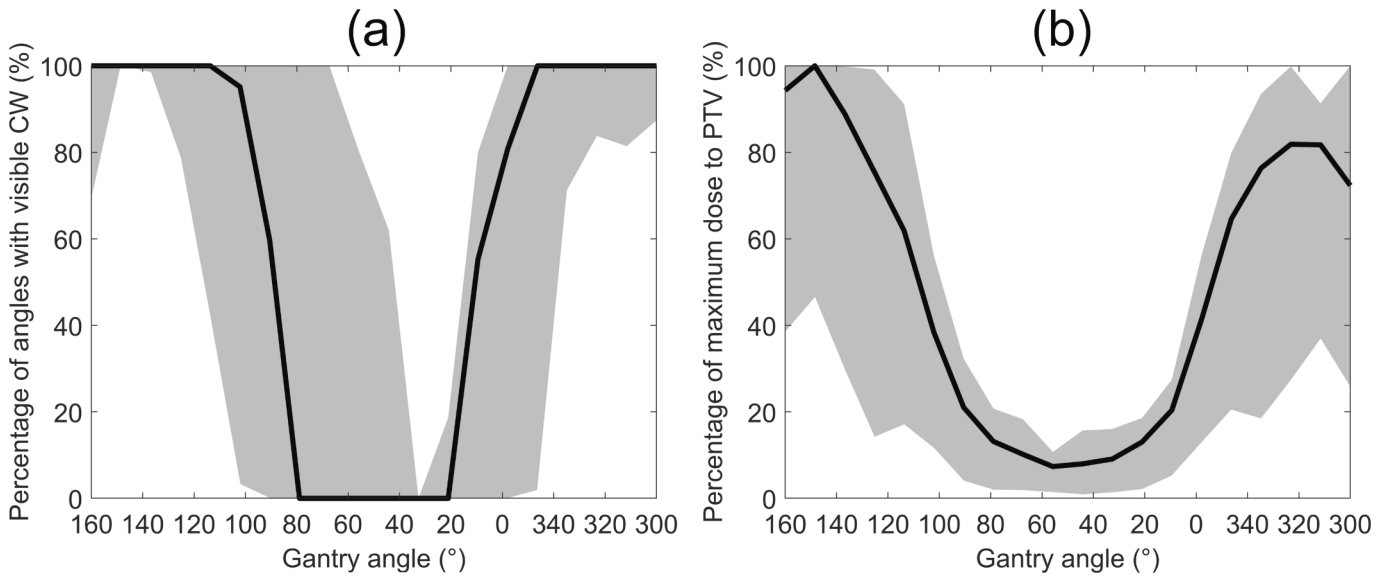

Fig. 2. (a) The median percentage of feasible gantry angles in each subarc over all 27 treatment arcs. (b) The median percentage of the maximum dose to the PTV over all treatment arcs. The shaded region denotes the data between the 10th and 90th percentiles.

Table 1
The RMS error for each shift in the position of the phantom, 5th and 95th percentile errors, along with the total number of frames captured in each arc.

Phantom Shift	Clockwise arc			Counter clockwise arc		
	RMSE (mm)	[5th,95th] percentile (mm)	Number of frames	RMSE (mm)	[5th,95th] percentile (mm)	Number of frames
Left-Right	0.4	[−0.5,0.6]	279	0.3	[−0.3,0.2]	335
Anterior-Posterior	0.5	[−0.3,0.9]	282	0.3	[−0.0,0.4]	339
Perpendicular to tangential angles	0.5	[−0.4,0.9]	281	0.3	[−0.2,0.4]	339
Parallel to tangential angles	0.4	[−0.2,0.6]	281	0.3	[−0.2,0.5]	300

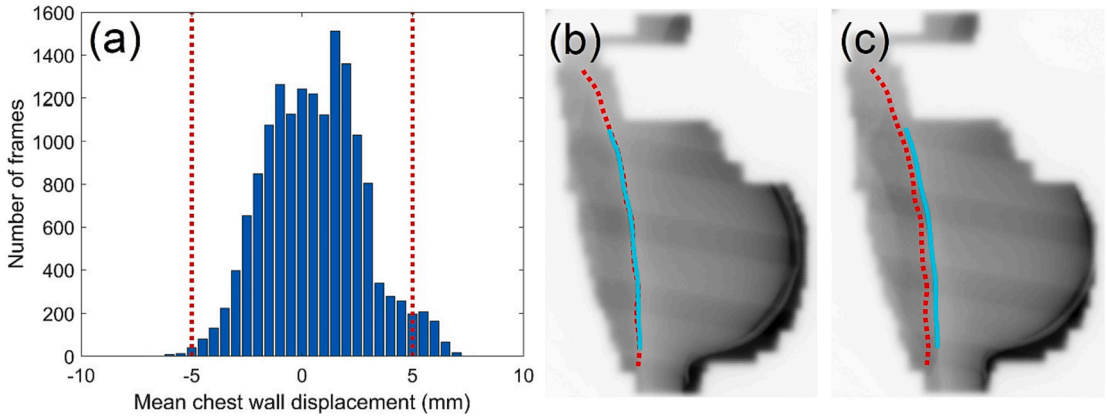

Fig. 3. (a) Distribution of measured mean CW displacements for all patients. A positive CW displacement denoted that the measured CW position was anterolateral of the planned position, while a negative value represented a posteromedial position. The red dotted lines represent the ±5 mm CTV-PTV margin thresholds. (b) An EPID frame for patient 04 with the CW position during treatment (light blue) well aligned to the planned position (red). (c) An EPID frame from another treatment arc for patient 04 in which the treatment and planned CW positions were misaligned. (For interpretation of the references to colour in this figure legend, the reader is referred to the web version of this article.)

DVH metrics increased by 12% and 42% for the $V_{10\%}$ and $V_{40\%}$, respectively. MHD increased by 36%.

4. Discussion

The chest wall monitoring software had sub-millimetre accuracy. The application of the method to breast VMAT patients was determined feasible, with the chest wall visible while a median value of 89% of the dose to the PTV was delivered. Hence it is likely that the software will detect errors in patient setup that are of dosimetric consequence.

The long tail in the mean CW displacement distributions for patient 04 and 10 (Fig. 4) were comprised of a small number of measured results that were identified via visual audit as inaccurate. These occurred in EPID images with poor image contrast resolution and may be omitted by increasing the minimum number of profiles per EPID image required for CW displacement calculation, or by using statistical analysis to detect

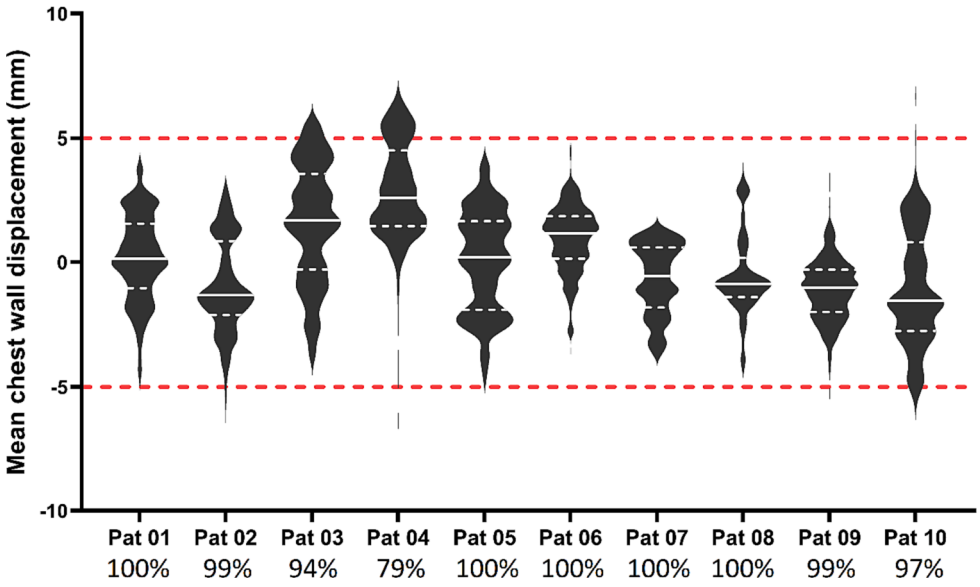

Fig. 4. A violin plot of the mean CW displacement per frame measured for each patient. CW displacements in the anterolateral direction are denoted as positive, while posteromedial CW displacements are negative. The unbroken white line represents the median displacement, the white dashed lines represent the 25th and 75th percentiles, and the red dashed lines represent the ±5 mm thresholds (i.e. CTV-PTV margin). The percentage of frames in which the CW displacement was found to be within the 5 mm threshold is listed underneath each patient.

outliers, either in each frame, or for each horizontal position over subsequent frames.

The mean CW displacement was found to be within the 5 mm CTV-PTV margin in 97% of time-resolved EPID measurements. While instances where the CW displacement was found to be larger than 5 mm were small (3%), it demonstrates occasions where the motion management strategy, based on an external surrogate, failed to ensure that the CW alignment remained within the CTV-PTV margin. Furthermore, the broad distribution of mean CW displacements for each patient (Fig. 4) highlights the variability in inter- and intrafraction CW alignment. This illustrates the value in utilising the chest wall monitoring software to identify and avoid systematic and random errors in real-time, including: uncertainty in the CBCT match during setup, poor correlation of the DIBH gating signal with internal CW anatomy [4]; and poor breath-hold reproducibility. This could potentially lead to reduced PTV margins.

The proposed method has the advantage of detecting geometric errors in target position directly (i.e. based on internal anatomy), with no added imaging dose contribution in a patient population where risk of secondary cancer is a concern. Surface-guided radiotherapy (SGRT) systems are commercially available for monitoring the breast tissue during radiotherapy without additional imaging dose [12,17], however, alignment errors observed by SGRT have been found to have a weak correlation with alignment errors observed in internal anatomy [15] and so cannot be used to replace a comprehensive image-guided radiotherapy regime [18]. 4DMRI studies have demonstrated intra-fraction motion of organs at risk [19] and complex motion of breast and nodal volumes [20].The combination of SGRT with real-time EPID monitoring would be complementary, allowing for simultaneous monitoring of the breast surface and internal anatomy on conventional linacs.

One avenue of future work is to reduce the computation time (currently ~2 s per frame) and adapt this method for use in an online capacity [21], allowing for potential intervention and repositioning of the patient during treatment. The measured CW displacement could also be combined with either offline [22] or real-time 4D dose reconstruction software [23] to better understand the dosimetric impact. Additionally, monitoring other features such as the breast tissue outline and the heart position is of great clinical interest [24].

In conclusion, a novel CW monitoring system has been developed and used to establish the feasibility of time-resolved EPID monitoring for breast VMAT DIBH with sub-millimetre accuracy. The method is applicable to any standard linac, and real-time implementation could be used to identify and prevent gross errors during treatment, as well as potentially reduce the planning target margins applied.

Declaration of Competing Interest

The authors declare that they have no known competing financial interests or personal relationships that could have appeared to influence the work reported in this paper.

Appendix A. Supplementary data

Supplementary data to this article can be found online at https://doi.org/10.1016/j.phro.2023.100419.

References

[1] Kurtz J. The curative role of radiotherapy in the treatment of operable breast cancer. Eur J Cancer 2002;38:1961–74.
[2] Darby SC, Ewertz M, McGale P, Bennet AM, Blom-Goldman U, Brønnum D, et al. Risk of ischemic heart disease in women after radiotherapy for breast cancer. N Engl J Med 2013;368:987–98.
[3] Desai N, Currey A, Kelly T, Bergom C. Nationwide Trends in Heart-Sparing Techniques Utilized in Radiation Therapy for Breast Cancer. Adv Radiat Oncol 2019;4:246–52.
[4] Doebrich M, Downie J, Lehmann J. Continuous breath-hold assessment during breast radiotherapy using portal imaging. Phys Imaging Radiat Oncol 2018;5:64–8.
[5] Fassi A, Ivaldi GB, Meaglia I, Porcu P, Tabarelli de Fatis P, Liotta M, et al. Reproducibility of the external surface position in left-breast DIBH radiotherapy with spirometer-based monitoring. J Appl Clin Med Phys 2014;15:4494.
[6] Lutz CM, Poulsen PR, Fledelius W, Offersen BV, Thomsen MS. Setup error and motion during deep inspiration breath-hold breast radiotherapy measured with continuous portal imaging. Acta Oncol 2016;55:193–200.
[7] Conroy L, Quirk S, Watt E, Ecclestone G, Conway JL, Olivotto IA, et al. Deep inspiration breath hold level variability and deformation in locoregional breast irradiation. Pract Radiat Oncol 2018;8:109–16.
[8] Cozzi L, Lohr F, Fogliata A, Franceschini D, De Rose F, Filippi AR, et al. Critical appraisal of the role of volumetric modulated arc therapy in the radiation therapy management of breast cancer. Radiat Oncol 2017;12:200.
[9] Fogliata A, Nicolini G, Bourgier C, Clivio A, De Rose F, Fenoglietto P, et al. Performance of a Knowledge-Based Model for Optimization of Volumetric Modulated Arc Therapy Plans for Single and Bilateral Breast Irradiation. PLoS One 2015;10:e0145137.
[10] Stanton C, Bell LJ, Le A, Griffiths B, Wu K, Adams J, et al. Comprehensive nodal breast VMAT: solving the low-dose wash dilemma using an iterative knowledge-based radiotherapy planning solution. J Med Radiat Sci 2022;69:85–97.
[11] Lamprecht B, Muscat E, Harding A, Howe K, Brown E, Barry T, et al. Comparison of whole breast dosimetry techniques - From 3DCRT to VMAT and the impact on heart and surrounding tissues. J Med Radiat Sci 2022;69:98–107.
[12] Rong Y, Walston S, Welliver MX, Chakravarti A, Quick AM. Improving intra-fractional target position accuracy using a 3D surface surrogate for left breast irradiation using the respiratory-gated deep-inspiration breath-hold technique. PLoS One 2014;9:e97933.
[13] Conroy L, Yeung R, Watt E, Quirk S, Long K, Hudson A, et al. Evaluation of target and cardiac position during visually monitored deep inspiration breath-hold for breast radiotherapy. J Appl Clin Med Phys 2016;17:25–36.

[14] Jensen C, Urribarri J, Cail D, Rottmann J, Mishra P, Lingos T, et al. Cine EPID evaluation of two non-commercial techniques for DIBH. Med Phys 2014;41:021730.
[15] Delombaerde L, Petillion S, Weltens C, Depuydt T. Spirometer-guided breath-hold breast VMAT verified with portal images and surface tracking. Radiother Oncol 2021;157:78–84.
[16] Offersen BV, Boersma LJ, Kirkove C, Hol S, Aznar MC, Biete Sola A, et al. ESTRO consensus guideline on target volume delineation for elective radiation therapy of early stage breast cancer. Radiother Oncol 2015;114:3–10.
[17] Delombaerde L, Petillion S, Michiels S, Weltens C, Depuydt T. Development and accuracy evaluation of a single-camera intra-bore surface scanning system for radiotherapy in an O-ring linac. Phys Imaging Radiat Oncol 2019;11:21–6.
[18] Cravo Sá A, Fermento A, Neves D, Ferreira S, Silva T, Marques Coelho C, et al. Radiotherapy setup displacements in breast cancer patients: 3D surface imaging experience. Rep Pract Oncol Radiother 2018;23:61–7.
[19] Habatsch M, Schneider M, Requardt M, Doussin S. Movement assessment of breast and organ-at-risks using free-breathing, self-gating 4D magnetic resonance imaging workflow for breast cancer radiation therapy. Phys Imaging Radiat Oncol 2022;22:111–4.
[20] Groot Koerkamp ML, van den Bongard HJGD, Philippens MEP, van der Leij F, Mandija S, Houweling AC. Intrafraction motion during radiotherapy of breast tumor, breast tumor bed, and individual axillary lymph nodes on cine magnetic resonance imaging. Phys Imaging Radiat Oncol 2022;23:74–9.
[21] Vasina EN, Kong N, Greer P, Baeza Ortega J, Kron T, Ludbrook JJ, et al. First clinical experience with real-time portal imaging-based breath-hold monitoring in tangential breast radiotherapy. Phys Imaging Radiat Oncol 2022;24:1–6.
[22] Poulsen PR, Schmidt ML, Keall P, Worm ES, Fledelius W, Hoffmann L. A method of dose reconstruction for moving targets compatible with dynamic treatments. Med Phys 2012;39:6237–46.
[23] Ravkilde T, Skouboe S, Hansen R, Worm E, Poulsen P. First online real-time evaluation of motion-induced 4D dose errors during radiotherapy delivery. Med Phys 2018;45.
[24] Poulsen PR, Thomsen MS, Hansen R, Worm E, Spejlborg H, Offersen B. Fully automated detection of heart irradiation in cine MV images acquired during breast cancer radiotherapy. Radiother Oncol 2020;152:189–95.